A&A 531, A57 (2011)
DOI: 10.1051/0004-6361/201016176

Astronomy & Astrophysics

RHESSI observations of long-duration flares with long-lasting X-ray loop-top sources

S. Kołomański, T. Mrozek, and U. Bąk-Stęślicka

Astronomical Institute of the University of Wrocław, Kopernika 11, 51-622 Wrocław, Poland
e-mail: [kolomans;mrozek;bak]@astro.uni.wroc.pl

Received 20 November 2010 / Accepted 20 April 2011

ABSTRACT

Context. The Yohkoh /HXT observations of long duration events (LDEs) have shown that the HXR emission (14−23 keV) is present for tens of minutes after flare maximum. As a result, some heating process is expected to exist during that time. The higher energy resolution of RHESSI compared to HXT allow us to analyse LDEs in a more comprehensive way.
Aims. We selected three LDEs observed by RHESSI to answer the questions of how long HXR emission can be present, where it is emitted, what its nature is and how much energy should be released to sustain the emission.
Methods. We used RHESSI data to reconstruct images of the selected flares with an energy resolution as high as 1 keV. Next we estimated physical parameters of HXR sources through imaging spectroscopy. The physical parameters obtained were then used to calculate the energy balance of the observed sources.
Results. We found that HXR thermal emission can be present for many hours after LDE flare maximum. The emission comes from large and hot loop-top sources. The total energy that must be released to sustain the emission of the sources is as high as 10^{31} erg.

Key words. Sun: flares – Sun: X-rays – gamma rays

1. Introduction

A long duration event (LDE) is a solar flare characterized by a slow decrease in soft X-ray (SXR) thermal emission. This decrease may last from several hours to more than a day. More insight into the nature of LDEs was gained from ultraviolet and X-ray observations during the Skylab, *SMM* (Solar Maximum Mission), and Yohkoh space missions (e.g. Sheeley et al. 1975; Kahler 1977; Feldman et al. 1995; Harra-Murnion et al. 1998; Czaykowska et al. 1999; Shibasaki 2002; Isobe et al. 2002). One of the most important conclusions is that, without the continuous energy input during the whole decay phase, LDEs would decay much faster than observed.

Loop-top sources (LTSs) are remarkable SXR and HXR (hard X-rays) features of solar flares seen close to a flare loop apex. They form before flare maximum, and in LDEs they may last many hours (e.g. Feldman et al. 1995; Kołomański 2007a). LTSs should be located close to the primary energy release site (e.g. Kopp & Pneuman 1976; Shibata 1999; Hirose et al. 2001; Karlický & Bárta 2006). Thus, they are a very promising tool for analysing of an energy release during the decay phase. LTSs were first recorded on images taken from Skylab and are commonly present in the Yohkoh/SXT flare observations. Since the first observation it has become clear that the presence of an LTS during the whole flare decay-phase requires continuous energy release and some restriction mechanism efficiently preventing outflow of mass and energy from an LTS (see Vorpahl et al. 1977). If not meeting these two requirements, loop-top sources would rapidly lose energy by radiative and conductive processes and would vanish. This result was later confirmed by an analysis based on RHESSI and Yohkoh data (e.g. Jiang et al. 2006; Kołomański 2007b).

In the CSHKP (e.g. Carmichael 1963; Hirayama 1974; Kopp & Pneuman 1976; Sturrock 1966) model of a solar flare, the energy release occurs above an LTS. This model and its numerous modifications (Krucker et al. 2008, and references within) successfully explain the observational features of solar flares observed in different wavelengths during the impulsive phase. However, the authors investigating LDEs (Nakajima et al. 1998; Uchida et al. 1999; Kundu & Grechnev 2001; Phillips et al. 2005) report observations that are inconsistent with the CSHKP concept. The main problems they had were related to non-thermal velocities of 20–50 km s^{-1}, the long times needed to keep the inflow of a magnetic field into a reconnection site and a lack of downflows or upflows. Recently Jiang et al. (2006) have investigated the heating and cooling processes of an LTS and find that there is a large amount of energy released during the decay phase of a short-duration solar flare. The authors suggest that in the case of an LDE the energy released during the decay phase may be even larger than the energy released during the impulsive phase.

An analysis of energy release during the decay phase can give us precise constraints for numerical flare models. The most demanding for the models is the long-lasting HXR emission from LTSs seen in LDE flares. Therefore such LTSs observed for many hours after a flare maximum are probably the most promising observational feature to set up the constraints. The sources should be very close to the energy release site and, as the most important attribute, they put high requirements on the energy release rate. If a long-lasting HXR source is thermal, then it must be continuously heated, because the characteristic radiative cooling time of hot (above 10 MK) and dense ($\approx 10^{10}$ cm^{-3}) plasma is ≈1 h. If an HXR source is non-thermal then there should be a continuous acceleration of particles, to counteract

Table 1. Basic information about the selected long-duration flares.

Flare	Date	Location		SXR flux maximum[3]		Duration[3]	Time intervals analysed
		active region[1]	coordinates[2]	time [UT]	class	[h]	beginning [UT] (duration [min])
LDE1	30 July 2005	10 792	N10E59	06:36	X1.3	11	10:20 (0.07), 11:30 (0.13), 11:55 (0.13), 12:40 (0.27), 13:34 (0.53), 14:15 (1.00), 15:55 (4.00), 16:26 (4.33)
LDE2	22 August 2005	10 798	S10W52	01:34	M2.7	11	01:35 (0.13), 01:55 (0.27), 02:45 (2.00), 03:24 (1.00), 04:22 (1.00), 04:46 (4.00), 05:56 (8.00), 06:36 (2.00), 07:29 (2.00), 08:08 (2.00)
LDE3	25 January 2007	10 940	S07E90	07:15	C6.3	17	07:03 (1.50), 07:55 (0.13), 08:12 (0.33), 08:32 (0.50), 09:30 (1.50), 09:50 (1.50), 10:10 (1.50), 11:00 (2.50), 11:22 (3.00), 11:47 (4.00), 12:30 (4.00), 12:56 (4.00)

Notes. [(1)] NOAA active region number; [(2)] heliographic coordinates; [(3)] according to GOES 1−8 Å database.

fast thermalization of non-thermal electrons. The timescale of the thermalization in the sense of momentum loss of electrons is about several seconds.

Hard X-ray LTSs have been reported before with Yohkoh/HXT data, but the observations were shorter than thermal soft X-ray LTSs. Masuda et al. (1998) observed HXR sources up to 30 min after flare maximum, with typical sizes 1–2 arcmin. Harra-Murnion et al. (1998) investigated two LDEs and concluded that HXR sources grow with time, with diameters ≈20–45 arcsec. In one of these flares the HXR source was visible up to 3 h after flare maximum. Kołomański (2007a,b) analysed three LDEs using Yohkoh data, finding that HXR sources during the decay phase are well correlated with SXR LTSs and were observed (in 14–23 keV range) for about 50 min after flare maximum. Khan et al. (2006) report the observation of a thermal HXR source lasting more than 1 h after flare maximum. In all these cases the HXR emission was observed close to and above the SXR emission source. Although Yohkoh/HXT data have provided useful information about LDEs, generally only the L channel (14–23 keV) shows significant emission for any length of time. It was thus not possible to distinguish between the thermal and non-thermal nature of an LTS.

Gallagher et al. (2002) observed evolution of an LTS using RHESSI and TRACE data. The HXR emission was observed in the 12–25 keV range some four hours after the flare maximum and almost 11 h in the 6–12 keV range. The LTS was large and its altitude increased at a speed that gradually declined from 10 to 1.7 $\mathrm{km\,s^{-1}}$. The higher energy emission (12–25 keV) was located above the lower energy ones (6−12 keV and 3–6 keV), and all HXR emission was located above the tops of the loops observed in the EUV range (TRACE 195 Å).

So far, most investigations of LDEs made with RHESSI have been restricted to a few wide (several keV) energy intervals. Recently Saint-Hilaire et al. (2009) have presented observations of a coronal source recorded by RHESSI. The source was observed for about 12 h in energies up to 10 keV. Emission of the the source was purely thermal with maximal temperature of about 11 MK. Authors estimated a total energy (about 4×10^{31} erg), which had to be deposited in the source to sustain its long-lasting emission.

Here we present the investigation of LDEs observed by RHESSI. The analysis is made using RHESSI images reconstructed in very narrow (1 keV) energy intervals. RHESSI is very useful for analysing weak sources, even with 1 keV energy resolution, thanks to its high spectral resolution. Thus, it gives an opportunity to determine the nature of LTSs emission – thermal or non-thermal. Using the images we estimated LTSs physical parameters through imaging spectroscopy. Then the parameters were used to calculate the energy balance of the observed sources and to find out how effective the energy release and heating processes are at the decay phase of an LDE.

2. Observations

Three LDEs, well observed by RHESSI (Lin et al. 2002), were selected for an analysis. We chose flares of significantly different powers and with decay phases lasting more than ten hours in GOES 1–8 Å range. The flares occurred on 30 July 2005 (hereafter the LDE1), 22 August 2005 (LDE2) and 25 January 2007 (LDE3). Basic information about the LDEs is given in Table 1. Our analysis is based on RHESSI data (Reuven Ramaty High Energy Solar Spectroscopic Imager, Lin et al. 2002) supported by SoHO/EIT (Extreme UV Imaging Telescope on-board the Solar and Heliospheric Observatory, Delaboudinière et al. 1995) and GOES/SEM (Space Environment Monitor on-board Geostationary Operational Environmental Satellites, Donnelly et al. 1977) observations.

2.1. On the RHESSI data

RHESSI is a rotating Fourier imager with nine detectors made of pure germanium crystals (Lin et al. 2002). The detectors record the energy and arrival time for each detected HXR photon. For strong solar flares the number of coming photons easily reaches 10^5 counts per second. As the number of counts rises, the lifetime of a detector decreases. The pulse pile-up (Smith et al. 2002) is the main problem connected with this effect. It occurs

when two or more photons arrive almost at the same time. In such a case the electronics of the detector recognize them as one photon with energy equal to the sum of these photons. When number of incoming photons is very high, the pulse pile-up may severely influence measured fluxes.

The number of HXR photons decreases strongly with energy, so problems with pulse pile-up occur mainly in the low-energy end of the range observed by RHESSI. Thus, to achieve the great dynamic range of the instrument, several systems were included to decrease the measured low-energy HXR photons. Among these systems are attenuators that are the most important source of uncertainty. The influence of the attenuators on measured fluxes is quite well understood at present, but in practice the attenuator could seriously complicate the spectral analysis (Smith et al. 2002), especially in the lowest energies.

For each orbit, RHESSI passes through the radiation belts and south Atlantic anomaly (SAA), which may also have a significant influence on the measured HXR fluxes. In our analysis we focused on the late phase of an LDE when the emission is extremely weak, so some care is needed in the analysis. However, the image spectroscopy has an advantage over standard spectroscopy based on fluxes measured for the whole Sun. The background photons do not influence modulation profile for the rotating Fourier imager. Thus, an analysis of very weak fluxes can be done much more easily than in the case of standard spectroscopy, especially for moments of passage through radiation belts when the background changes very quickly with time.

RHESSI light curves of the LDEs are shown in Figs. 3, 8, and 12. The effect of radiation belts and SAA passages can be seen on the light curves. Usually the SAA influence is observed as a rise in the signal observed several minutes before and after the passage. When satellite is in the SAA detectors are switched off. The influence of the radiation belts is visible as a slow oscillation of the signal.

3. Analysis

3.1. Imaging

It is a large difficulty to reconstruct a RHESSI image when an emitting source is weak. Usually RHESSI image reconstruction is performed for detectors nos. 3–6, 8, 9. Depending on the reconstruction algorithm and weights chosen, this set of detectors gives a spatial resolution of about 7−9 arcsec (Aschwanden et al. 2002). However, we were not able to reconstruct any reliable image in a case of very late phase of LDE decay with the use of this standard set of grids. The weak signal was not the problem since by taking integration times up to 8 min we were able to collect enough counts, i.e. about several thousand.

The problem may be solved if we remember that when the source size is comparable to the resolution of a particular grid, then the detector records very weak or no modulation of the signal (Hurford et al. 2002). The resulting image obtained for this grid is then dominated by noise. This grid added to the set used for reconstruction only introduces noise. In the worst case we may not get convergence of the reconstruction algorithm.

We tried to solve this problem in the following way. First, we reconstructed images for single grids and a wide field of view (8 arcsec pixel, image size 256 × 256 pixels) using the back-projection algorithm (Hurford et al. 2002). Next, we used these images for determining which grid provides us with reliable images of the source. An example is presented in Fig. 1. For some time intervals there is only noise in the narrow grids, although count rates are high. Taking this into account, we selected, for a given time interval, only those grids that showed a definite source in a single detector image.

In the next step we used chosen set of grids to reconstruct images with a PIXON algorithm (Puetter & Yahil 1999, and references within). Since integration times are rather long (minutes) we used stacked modulations[1]. Images obtained with this method were stabler than without it. Stabler means that images were similar in neighbouring time and energy intervals. Moreover there were fewer images where we did not get convergence of the reconstruction algorithm. The energy resolution chosen for reconstruction was as narrow as possible, i.e. 1 keV. It enabled us to obtain reliable fits to observed spectra.

3.2. Geometrical properties – LTS centroid location, altitude and size

Having reconstructed set of images we were interested in obtaining some properties of observed sources. In each image we determined sources using 50% of the brightest pixel intensity isoline. In each case we observed sources only related to coronal parts of flaring structure (loop-top sources). There was no observed emission localized on the chromosphere level (footpoint sources), which is rather typical for the decay phase of an LDE.

We determined position of loop-top sources by finding their centroids. The centroids were estimated as centres of gravity of the emission within the 50% intensity isoline (relative to the brightest pixel in the RHESSI image). The uncertainty of the source location estimation is caused by two agents. The first agent is an uncertainty connected with the spatial resolution of the instrument, although by using centroids we significantly improved the accuracy of source location estimation with regard to nominal. In our analysis this error was always less than 1.5 arcsec. More uncertainty was produced by the behaviour of analysed sources. We often observed a systematic trend in source location: the higher the energy of the source, the higher it was observed in the corona. Such a systematical effect should be considered when estimating an actual source position. Thus, for a particular time interval we measured a spread of values obtained for different energies, and the spread was assumed to be a good approximation of uncertainty in source position. We usually obtained values of about 5 arcsec. This systematic trend (higher energy = higher altitude) is a common observational phenomenon (e.g. Gallagher et al. 2002; Sui & Holman 2003; Liu et al. 2008; Saint-Hilaire et al. 2009). Usually centroids of a source in energies below 10 keV are up to several arcsec below centroids in energies about 20 keV.

To estimate the altitude of an LTS we need to know its position in the RHESSI image and find the point on the solar photosphere above which the source is situated (reference point). The source position was defined, as mentioned, by the position of its centroid. The position of reference point was taken from locations of foot point sources observed by RHESSI at impulsive phase (LDE1), the locations of flare ribbons recorded by SoHO/EIT (LDE2) and the method described by Roy & Datlowe (1975) (LDE3). The method allowed estimating heliographic coordinates for flares behind the solar limb. We plotted a position (on the solar disk) of an active region in which an analysed, behind-the-limb flare occurred as a function of time. The position was taken from the positions of all on-disk flares that occurred in that active region. Then we extrapolated the position

[1] http://sprg.ssl.berkeley.edu/~tohban/nuggets/?page=article\&article_id=39

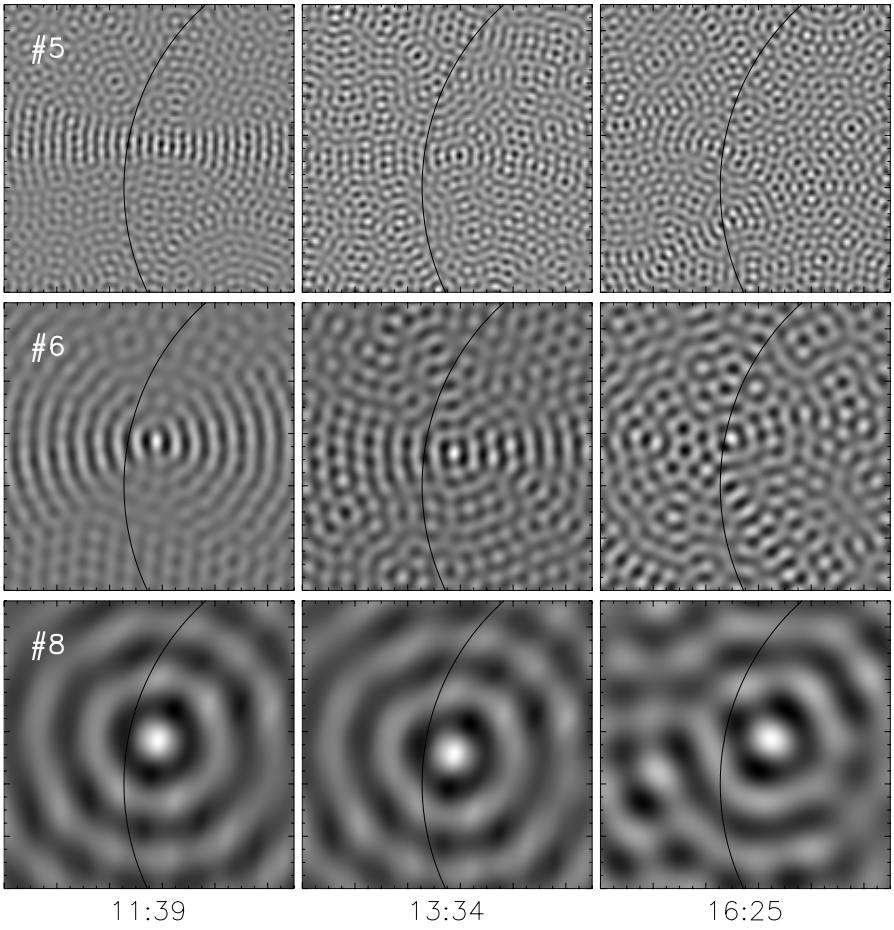

Fig. 1. The 6–7 keV back-projected RHESSI images reconstructed for selected grids (Nos. 5, 6, 8) and three time intervals (the 30 July 2005 flare). When a source size is comparable to the resolution of a particular grid, the image obtained for this grid is dominated by noise. Field of view of each image is 1024 × 1024 arcsec. The Sun limb is marked be a black line.

vs. time plot behind the limb to get a position of our behind-the-limb flare.

Since a moment of time for which the position of the reference point was determined is different from the analysed time intervals, all the positions were corrected to account for the solar rotation. Finally, the LTS altitude was calculated as the distance between its centroid and the reference point. The altitudes obtained were corrected for the projection effect. Errors in the location of reference point and the location of source centroid were included in the altitude errors. The relative error in the altitude is about 10 percent.

The actual size of an LTS was determined using PIXON images reconstructed with the use of all detectors in which we observed the source at a given time. The size of the source was estimated as the FWHM size. We did not observe important and systematic change in source size with energy. Thus, we decided to use PIXON images reconstructed in the energy interval 7–8 keV for the estimation of a source size.

3.3. Imaging spectroscopy of an LTS

The main motivation for reconstructing images in narrow energy bands is the spectroscopy of the spatially resolved HXR sources. For this purpose we used the OSPEX[2] package. The HXR continuum was fitted with thermal and non-thermal components, if observed. We usually also observed line features at 6.7 keV and 8 keV (Phillips et al. 2006). The physical parameters of observed sources were obtained from fits. Namely, for each time interval we obtained temperature and emission measure (thermal emission). If a non-thermal component was observed then we fitted it with double power-law function. We treated a break energy and power-law index above this energy as free parameters. The power-law index below the break energy was fixed at a constant value equal to zero.

3.4. Energy balance

As mentioned in the introduction, the presence of HXR emission from an LTS during the decay phase is evidence of energy release at that time. To calculate the heating rate of an LTS we considered its energy balance during the decay phase. Three major cooling processes were included in this balance: expansion, radiation, and conduction,

$$\left(\frac{\mathrm{d}\mathcal{E}}{\mathrm{d}t}\right)_{\mathrm{obs}} = \left(\frac{\mathrm{d}\mathcal{E}}{\mathrm{d}t}\right)_{\mathrm{ad}} - E_{\mathrm{C}} - E_{\mathrm{R}} + E_{\mathrm{H}}, \quad (1)$$

where

- $\mathcal{E} = 3NkT$ is thermal energy density;
- $\left(\frac{\mathrm{d}\mathcal{E}}{\mathrm{d}t}\right)_{\mathrm{obs}}$ is the decrease in $\mathcal{E}$ per second estimated from temperature (T) and density (N) values;
- $\left(\frac{\mathrm{d}\mathcal{E}}{\mathrm{d}t}\right)_{\mathrm{ad}}$ is the decrease due to the adiabatic expansion of plasma in a source;
- E_{C} is the energy loss due to thermal conduction;
- E_{R} is the radiative loss; and
- E_{H} is the heating rate or thermal energy release.

[2] http://hesperia.gsfc.nasa.gov/ssw/packages/spex/doc/ospex_explanation.htm

The values of E_C, E_R, and E_H are in erg cm^{-3} s^{-1}. We calculated

- $\left(\frac{d\mathcal{E}}{dt}\right)_{ad} = 5kT\left(\frac{dN}{dt}\right)$;
- $E_C = 3.9 \times 10^{-7} T^{3.5}/(Lr)$ where r is the LTS radius and L is loop semi-length (assuming that energy is conducted to the chromosphere, Jakimiec et al. 1997); and
- $E_R = N^2\Phi(T)$ where $\Phi(T)$ is the radiative loss function taken from Dere et al. (2009).

We took the altitude of an LTS above the photosphere (h) as an approximation for L in the expression for E_C. Of course, h is smaller than L, but they do not differ too much. From Eq. (1) we calculated upper and lower limits for E_H. The upper limit, $(E_H)_{max}$, is calculated directly from Eq. (1) i.e. with E_C described by Spitzer thermal conduction (Jakimiec et al. 1997). However, it has been shown that the actual conductivity may be lower than Spitzer conductivity (Luciani et al. 1983). A lower (the lowest possible) limit, $(E_H)_{min}$, can therefore be obtained assuming $E_C = 0$, though this may not be physically realistic. The actual value of LTS heating rate must be contained between the upper and lower limits of E_H.

3.5. Diagnostic diagram

We used diagnostic (temperature-density, $T - N$) diagrams as an independent tool for analysing energy release. The method of investigating flare evolution by temperature-density diagrams was put forward by Jakimiec et al. (1986, 1987, 1992) and Sylwester et al. (1993). It was shown that temporal evolution of flares does not depend much on their morphology. Thus, the diagrams allow us to study temporal changes in the energy release in flares qualitatively (Jakimiec & Fludra 1992). Jakimiec et al. (1992) in their hydrodynamic modelling considered a single, symmetrical loop with constant cross-section and constant heating rate before a flare. The authors took the following variation of the heating rate with time t in their calculations:

$$E_H(t) = \begin{cases} A = \text{const.} & \text{for } 0 < t < t_1 \\ Ae^{-\frac{t-t_1}{\tau}} & \text{for } t > t_1. \end{cases} \quad (2)$$

They studied two evolutionary tracks with $\tau = 0$ s and $\tau = 300$ s for a flaring loop of semi-length $L = 2 \times 10^4$ km.

Non-flaring, steady loops having the same semi-length L but different temperature T and density N lie along a straight line (the line of steady state loops, S-S line). Dependence between T and N for the S-S coronal loops is described by the scaling law (Rosner et al. 1978):

$$T = 6.9 \times 10^{-4}(NL)^{1/2}. \quad (3)$$

The inclination of the S-S line is $\xi = \frac{d\log T}{d\log N} \approx 0.5$. A flare evolution on the diagnostic diagram can be divided into a few stages (see Fig. 2).

1. AB – Point A, lying on the S-S line, represents pre-flare conditions in a loop. The heating rate is constant, and the loop is in steady-state. At the beginning of the flare energy is released abruptly causing an increase in temperature (path AB).
2. BC – Temperature is constant, electron density increases gradually due to chromospheric evaporation. Rate of energy release starts to decreases at point C.

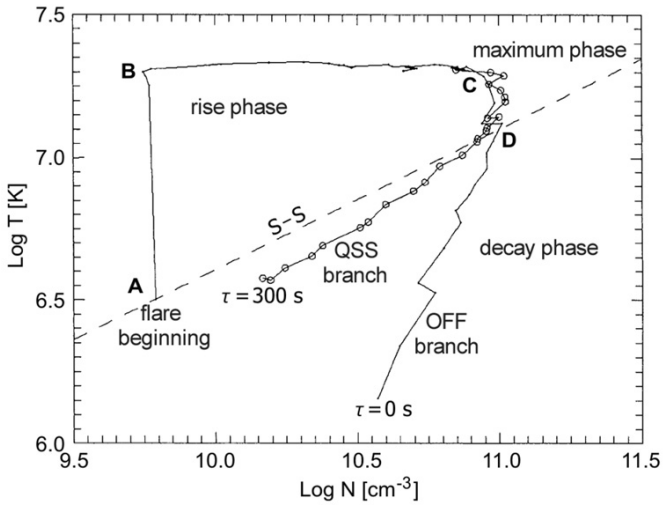

Fig. 2. Density-temperature diagnostic diagram illustrating the dependence of the slope on the characteristic decay time of the heating rate ($\tau = 0$ s and $\tau = 300$ s cases are shown). The figure comes from Jakimiec et al. (1992).

3. CD – Decreasing heating rate (point C) causes decrease in the temperature. However, the temperature is still high enough to cause more chromospheric evaporation and to increase the electron density (path CD). When released energy becomes insufficient the density in the loop begins to decrease (near the line S-S, point D).

Evolution of a flare during the decay phase depends on how fast the heating rate E_H decreases. In calculations two boundary scenarios observed during the decay phase may be present.

- If E_H decreases very fast, with an e-folding decay time shorter than the thermodynamic decay time $\tau_{th} \propto L/\sqrt{T_0}$ (L – semilength of a loop, T_0 – initial temperature at the top of a flaring loop), then the flare evolves along the OFF branch (E_H switched-off evolution). The evolution is characterized by a fast decrease in T caused by the loop cooling owing to thermal conduction losses and radiative losses not balanced by the heating rate, which is too low. This evolution is represented in Fig. 2 by a branch for E_H e-folding decay time $\tau = 0$ s.
- If E_H decreases slowly, with τ longer than τ_{th}, the flaring loop will go through a sequence of steady-state configurations. In a $T - N$ diagram, such a flare evolves along the QSS branch (quasi-steady-state evolution), which is parallel to the S-S line. During the QSS evolution, T drops slower than for the OFF evolution because the thermal conduction and radiative losses are balanced by the heating rate, which is high enough. The QSS evolution is shown in Fig. 2 by a branch for the E_H e-folding decay time $\tau = 300$ s.

These results were obtained for a loop with a constant length. However, observations show that the height of flaring loops usually increases during a flare evolution. If density also decreases (which is typical of solar flares), then QSS path will have a smaller inclination than 0.5 (see Kołomański 2007b). In typical LDEs this altitude-density factor can lower the inclination of QSS path by about 0.1–0.2.

The time behaviour of the energy release during the decay phase of the analysed flares was investigated using simplified diagnostic diagram ($\log T$ vs. log EM) obtained from the GOES/SEM data. The diagnostic diagrams obtained are shown in Figs. 7, 11, 15.

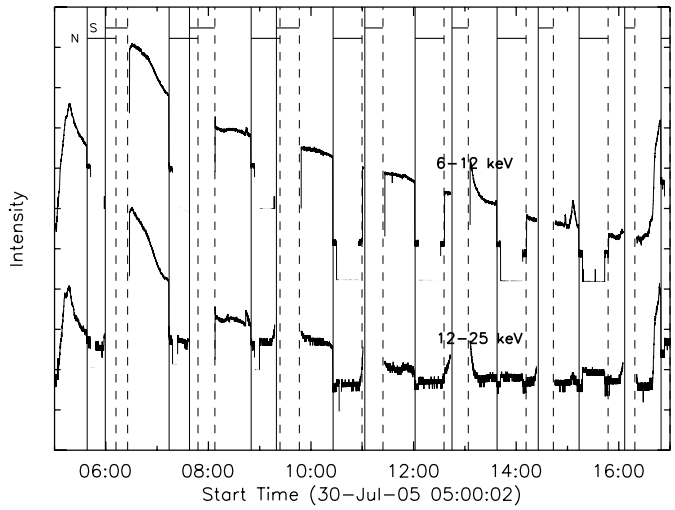

Fig. 3. RHESSI light curves for the 30 July 2005 flare. Vertical lines mark the boundaries of the satellite night (N) and the south Atlantic anomaly (S) periods (solid and dashed lines mark the beginnings and ends of the periods, respectively). The light curves were shifted vertically for clarity. The intensity is given in relative units.

4. Results

4.1. The 30 July 2005 flare

RHESSI light curves of the LDE1 are shown in Fig. 3. The flare emission could be analysed for eight intervals, given in Tables 1 and 2. In the lower standard energy range 6 to 12 keV, RHESSI recorded the emission for ten hours during the decay phase until the beginning of the next flare. In the higher energy range 12 to 25 keV, the emission was detectable for six hours after flare maximum.

Appearance of the flare and its evolution are shown in Fig. 4. The figure presents EIT 195 Å images with a source observed by RHESSI overlaid. As can be seen in EUV the LDE1 consisted of several loops forming an arcade. In X-rays there was one loop-top source located just above the arcade of loops.

The basic geometrical and physical properties of the loop-top source are given in Table 2. The LTS size was about 32−35 arcsec in diameter, and it did not change significantly with time. The LTS had an elliptical shape with a longer axis running along the tops of the loops. The loop heights and LTS altitude slowly increased. The altitude grew from 47 $\times$ 10^3 to 60 $\times$ 10^3 km with an average velocity of 1 km s^{-1}. The LTS spectrum could be fitted with one thermal component for all time intervals except for the three earliest ones for which we had to use a second component. The best fit was obtained for a thermal component with a power-law component (see Fig. 5, see the conclusions for details).

Estimated values of LTS heating rate are shown in Fig. 6. The actual value of the heating rate is about 0.1−0.01 erg cm^{-3} s^{-1}. The non-zero value of E_H is confirmed by a diagnostic diagram (see Fig. 7). The decay path of the flare runs along the QSS path; i.e., there was continuous release of the energy, and the rate of the release decreased very slowly, which resulted in very slow cooling of LTS plasma. The characteristic time of temperature decrease was about eight hours.

Table 2. Basic parameters of the loop-top source of the 30 July 2005 flare.

Time [UT]	Size (diameter) [arcsec]	Altitude [10^3 km]	Temperature [MK = 10^6 K]	Emission measure [10^{47} cm^{-3}]
10:20	42.2	47.5	11.2	9.90
11:30	34.4	54.0	10.0	8.04
11:55	34.8	52.9	9.3	9.01
12:40	35.4	56.0	8.9	6.11
13:34	24.4	58.0	8.0	6.85
14:15	33.0	60.4	7.6	5.23
15:55	32.0	59.5	7.9	1.31
16:26	25.8	58.2	8.2	0.78

4.2. The 22 August 2005 flare

RHESSI light curves of the LDE2 are shown in Fig. 8. The flare emission could be analysed for ten intervals (see Tables 1 and 3). In the lower energy ranges 6 to 12 keV, RHESSI recorded the emission for seven hours during the decay phase until a two-hour gap in the satellite data. In the higher range 12 to 25 keV, the emission was detectable for three hours after flare maximum.

Images of the flare and its evolution are shown in Fig. 9 (EIT 195 Å images with LTSs observed by RHESSI overlaid on). The LDE2 was visible as an arcade of loops in EUV, while in X-rays there was three loop-top source located just above the arcade. The first two sources (LTS1, LTS2) were visible for about 4.5 h until 6 UT. The third LTS appeared just before 6 UT and was present at least until the end of observations, i.e. for over two hours. The LTS1 and LTS2 were not separated well enough to be analysed individually, therefore we treated them as one source denoted as LTS1-2.

Basic geometrical and physical properties of the loop-top sources are given in Table 3. The LTS1-2 size grew from about 30 to 50 arcsec in diameter, while the LTS3 size remained almost unchanged (40 arcsec, excluding the last observation point). The three loop-top sources were located along the tops of the loops. The altitude of the LTS1-2 grew from 31 $\times$ 10^3 to 65 $\times$ 10^3 km with an average velocity of 2 km s^{-1}. The LTS3 was located higher but is moved upwards with velocity two times lower. The emission of each LTS could be well described by a single thermal component for the whole decay phase.

The heating rates of LTS1-2 and LTS3 are shown in Fig. 10. E_H was non-zero and slowly decreased with time as can be seen. This temporal behaviour of the heating rate is confirmed by the diagnostic diagram (see Fig. 11). The decay branch of the flare runs along the QSS path or even flatter (due to the altitude-density factor). The characteristic times of temperature decrease were about six hours for LTS1-2 and seven hours for LTS3.

4.3. The 25 January 2007 flare

RHESSI light curves of the LDE3 are shown in Fig. 12. The flare emission could be analysed for twelve intervals (see Tables 1 and 4). In the energy range 6 to 12 keV, RHESSI recorded the emission for six hours during the decay phase until a two-hour gap in the satellite data. In the higher range 12 to 25 keV, the emission was detectable for one hour after the LDE3 maximum.

Figure 13 shows images of the LDE3 during its decay phase (EIT 195 Å images with intensity isolines from RHESSI). The LDE3 was a limb arcade flare with only footpoints obscured by the solar disk (see EIT images). The X-ray emission came from a

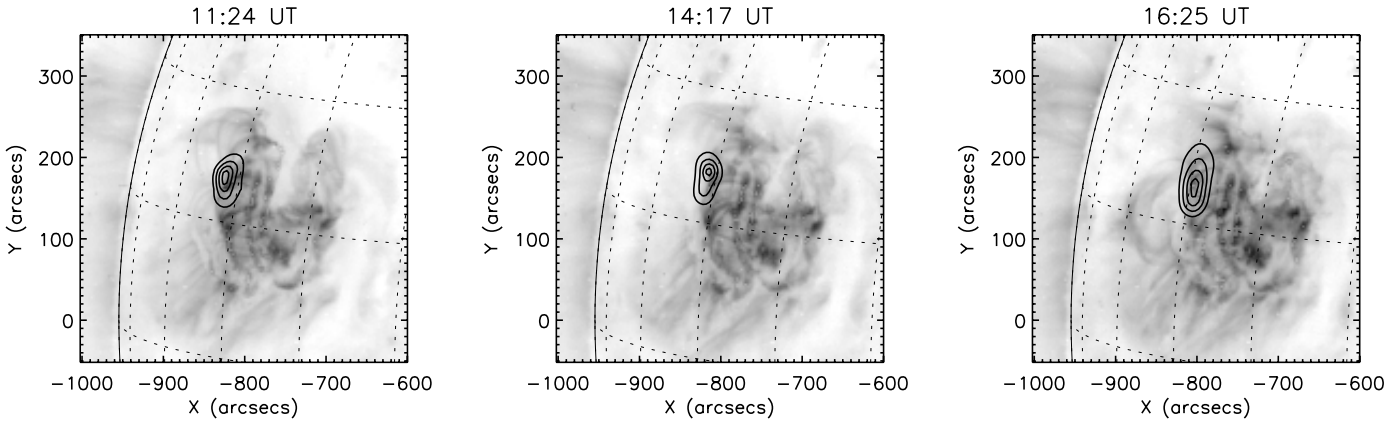

Fig. 4. SoHO/EIT 195 Å images illustrating the decay phase of the 30 July 2005 flare. Contours show the emission in the 7–8 keV range observed with RHESSI.

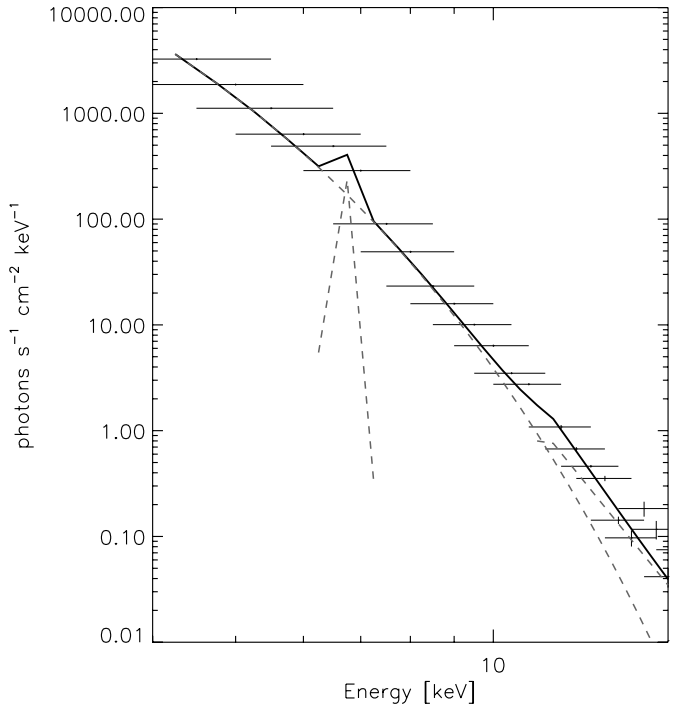

Fig. 5. RHESSI X-ray spectrum for the loop-top source of the 30 July 2005 flare recorded at 11:30 UT (horizontal bars, the bars widths corresponds to the energy bands widths). This spectrum was fitted using the thermal component, power-law, non-thermal component and the spectral line complex at 6.7 keV (grey dashed lines). The total fitted model is marked by a black line.

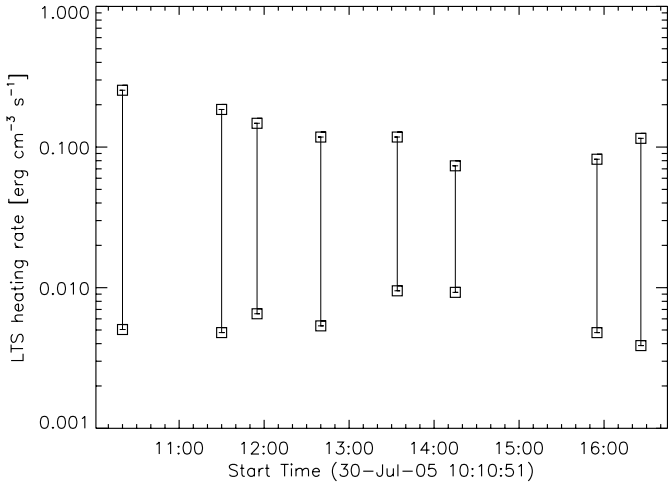

Fig. 6. The 30 July 2005 flare – estimated range of the heating rate of the loop-top source. The real value of the heating must be contained between the upper (upper symbols) and lower (lower symbols) limits of the heating rate.

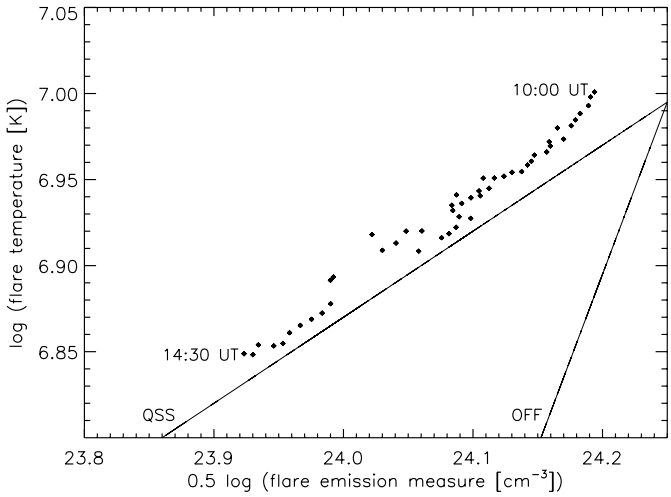

Fig. 7. GOES diagnostic diagram for the 30 July 2005 flare. The OFF and QSS paths of evolution are marked. The flare decay path runs along the QSS path. This confirms non-zero, slowly decreasing heating during the decay phase of the flare.

source located just above EUV loops. In some energies and time intervals there were two LTSs, but there was too few such observational points to analyse both LTSs separately, so we decided to treat them as one source.

Basic geometrical and physical properties of the loop-top source are given in Table 4. The LTS diameter changed from about 30 arcsec to 40 arcsec, while its altitude grew from about 30×10^3 to 75×10^3 km with an average velocity of 2 kms^{-1}. The emission of the LTS could be described well by a single thermal component for all time intervals.

The heating rate of the LTS of LDE3 are shown in Fig. 14, where E_H is non-zero and slowly decreased with time. This

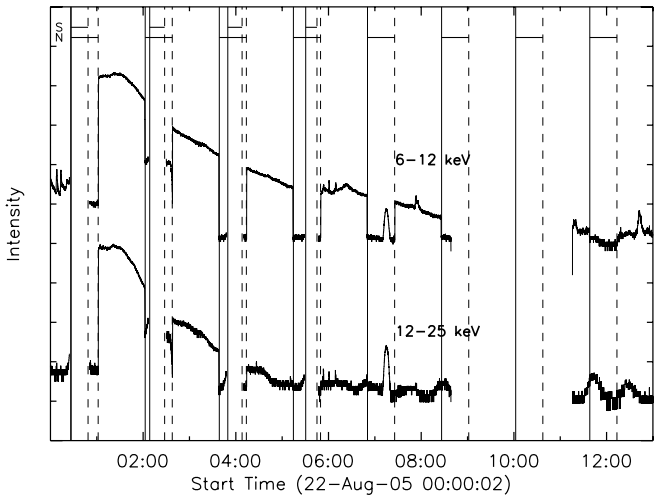

Fig. 8. RHESSI light curves for the 22 August 2005 flare. Vertical lines mark the boundaries of the satellite night (N) and the SAA (S) periods (solid and dashed lines mark the beginnings and ends of the periods, respectively). The light curves were shifted vertically for clarity. The intensity is given in relative units.

Table 3. Basic parameters of the loop-top sources of the 22 August 2005 flare.

Time [UT]	Size (diameter) [arcsec]	Altitude [10^3 km]	Temperature [MK = 10^6 K]	Emission measure [10^{47} cm^{-3}]
LTS1-2				
01:35	28.4	31.1	19.4	29.81
01:55	31.8	33.4	15.6	35.12
02:45	37.0	36.5	11.9	18.54
03:24	37.2	42.6	12.3	7.26
04:22	41.8	51.2	11.1	3.40
04:46	53.6	57.4	10.1	3.20
05:56	45.8	65.3	9.9	1.01
LTS3				
05:56	42.4	75.8	12.4	0.23
06:36	39.0	78.0	11.1	0.82
07:29	41.2	83.0	9.2	0.71
08:08	62.8	78.6	9.9	0.85

temporal behaviour of the heating rate is confirmed by the diagnostic diagram (see Fig. 15). The decay branch of the flare runs along the QSS path or even flatter (due to the altitude-density factor). The characteristic time of temperature decrease was very long, 21 h.

5. Conclusions

Previous results of the investigation of long-lasting HXR sources were based on the data giving rough information for the physical parameters of a source. The Yohkoh HXT L channel gave an integrated flux in the wide energy band, 14 to 23 keV. Using the RHESSI data we are now able to analyse the HXR flux and images with as energy resolution as good as 1 keV. We analysed RHESSI images and spectral data for the three selected long-duration flares, which occurred on 30 July 2005, 22 August 2005, and 25 January 2007.

The flux for energy above 12 keV was detected for six, three and one hours during the decay phase of LDE1, LDE2, and LDE3, respectively. Below 12 keV emission was observed for at least ten, seven and six hours after maximum of LDE1, LDE2, and LDE3, respectively. Such long-lasting, high-energy emission is the first perceptible circumstantial evidence of any heating processes during the decay phase.

For all analysed LDEs and all time intervals, we observed large hard X-ray loop-top sources. Each LTS observed was smooth, without any internal structure despite the high angular resolution of RHESSI (better than 10 arcsec). No LTS was visible in images reconstructed for a single narrower grid number 1−4 (angular resolution 2.3−12 arcsec), so a large LTS cannot be explained as a superposition of smaller unresolved subsources unless separations of the subsources is smaller than angular resolution of the finest RHESSI grid (2.3 arcsec).

The emission of the LTSs can be described as a single thermal component for almost all time intervals. Temperature of the component was quite high (more than 10 MK in the early part of the decay phase) and decreased very slowly. A characteristic time of the decrease was at least six hours, which is several times longer than a characteristic time for radiative cooling. A characteristic time for Spitzer conductive cooling is up to several minutes. This is indirect but strong evidence that efficient heating of LTSs is needed to enable their long-lasting existence.

This conclusion is confirmed by an energy balance calculation. The actual value of E_H is higher than zero in all analysed time intervals, implying that the energy release occurred many hours after the flare's maximum. The total amount of thermal energy released during the decay phase is big and is about 10^{31} erg cm^{-3} s^{-1}. This is a large amount of energy and it can be comparable to or even greater than the amount of energy released during the impulsive phase of a flare (see Jiang et al. 2006). Non-zero, slowly decreasing heating during the decay phase was confirmed independently by the analysis of diagnostic diagrams. The decay evolution path runs along the QSS line or is sometimes even flatter (due to altitude-density factor) for each of the three LDEs.

Similar results concerning the energy release during the decay phase of LDEs were obtained in analysis based on Yohkoh/SXT data (e.g. Isobe et al. 2002; Kołomański 2007b). However, RHESSI data enable us to estimate much more reliable value of plasma temperature – the SXT telescope had limited sensitivity to hot plasma, so the values for the temperature and therefore heating rate obtained from RHESSI data are higher than those obtained earlier from the SXT data. A proper solar flare model should be able to explain these more severe results.

In the case of LDE1 for the three earliest time intervals, the emission of LTS cannot be described by a single spectral component regardless of the simple structure of the source. The analysis of spatially resolved spectra of the LDE1 showed that LTS emission at that time consisted of two qualitatively different spectral components. The best fit to the observed spectra was obtained for a thermal component plus a power-law component with index $\gamma = 9.7$ and break energy equal to 12 keV. A slightly worse fit was obtained for two thermal components. This result puts some requirements on solar flare models regardless of the nature of the second component. If both components are thermal, some mechanism should exist that limits fast mixing of hotter and cooler plasma in an LTS. Moreover, the hotter component should be continuously heated by some mechanism. If one component is thermal and second is non-thermal, an acceleration process occurring within the hot (10 MK) and dense (10^9−10^{10} cm^{-3}) region is needed. Both cases could be explained well by MHD turbulence in an LTS region. The turbulence produces a large amount of small-scale reconnection

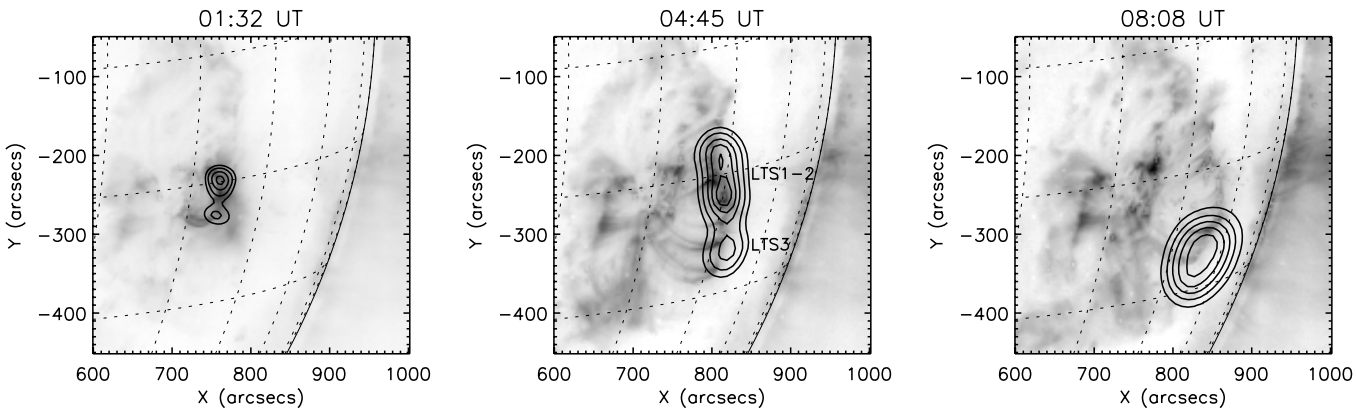

Fig. 9. SoHO/EIT 195 Å images illustrating the decay phase of the 22 August 2005 flare. Contours show the emission in the 7–8 keV range observed with RHESSI.

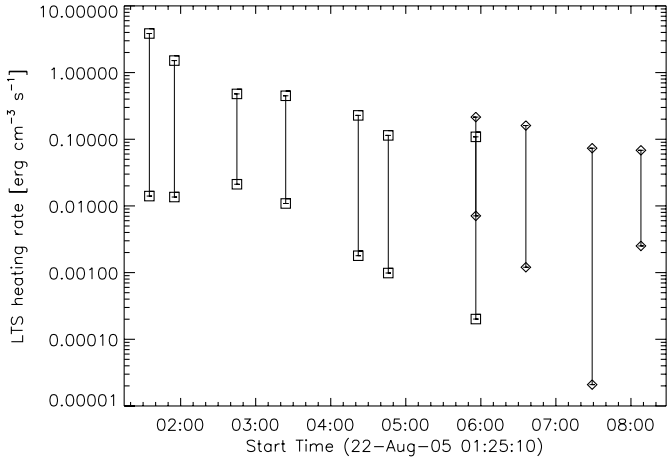

Fig. 10. The 22 August 2005 flare – estimated range of the heating rate of the LTS1-2 source (squares) and LTS3 source (diamonds). The real value of the heating must be contained between the upper (upper symbols) and lower (lower symbols) limits of the heating rate.

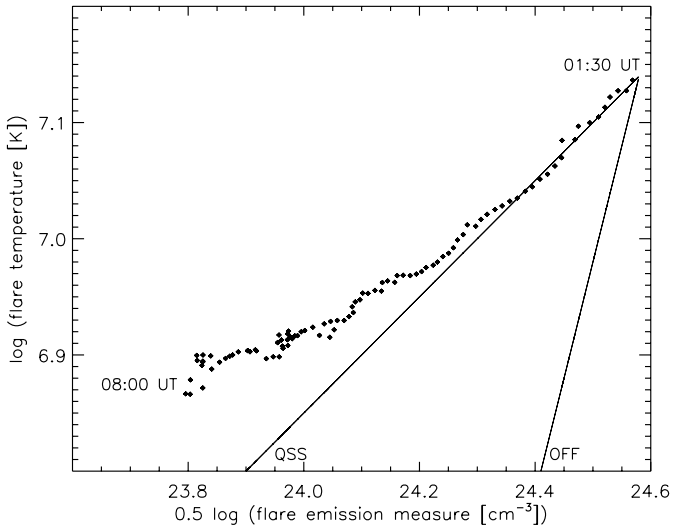

Fig. 11. GOES diagnostic diagram for the 22 August 2005 flare. The OFF and QSS paths of evolution are marked. The flare decay path runs along the QSS path (or even flatter). This confirms non-zero, slowly decreasing heating during the decay phase of the flare.

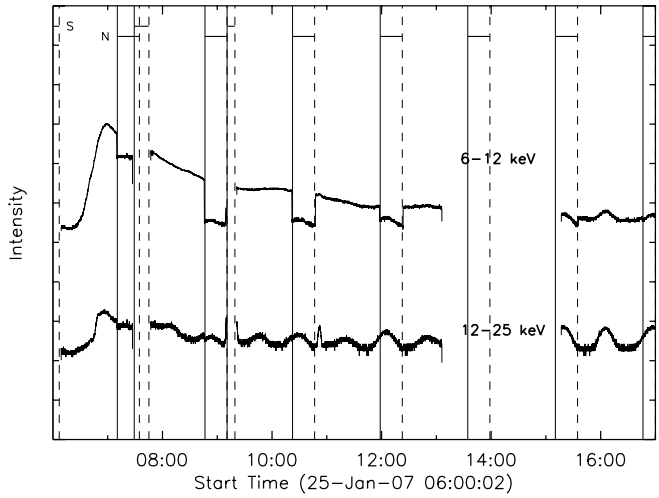

Fig. 12. RHESSI light curves for the 25 January 2007 flare. Vertical lines mark the boundaries of the satellite night (N) and the SAA (S) periods (solid and dashed lines mark the beginnings and ends of the periods, respectively). The light curves were shifted vertically for clarity. The intensity is given in relative units.

regions where magnetic energy is continuously converted into thermal and non-thermal energy of plasma. Turbulence can also impede the escape of thermal energy generated by these small-scale reconnection regions outside, since in coronal conditions turbulent conductivity may be several orders of magnitude lower than classical thermal conductivity parallel to magnetic field lines. The MHD turbulence inside LTSs has been proposed by several authors (e.g. Jakimiec et al. 1998; Jiang et al. 2006; Kontar et al. 2011). A different explanation of two distinct thermal components observed within a flare coronal source was proposed by Caspi & Lin (2010). These authors have performed an analysis of the 23 July 2002 flare close to its maximum (the whole rise phase, maximum and the first part of the decay phase) and concluded that the hotter (20 to 40 MK) component comes directly from coronal reconnection region, while the cooler component (≤20 MK) originates mainly from chromospheric evaporation.

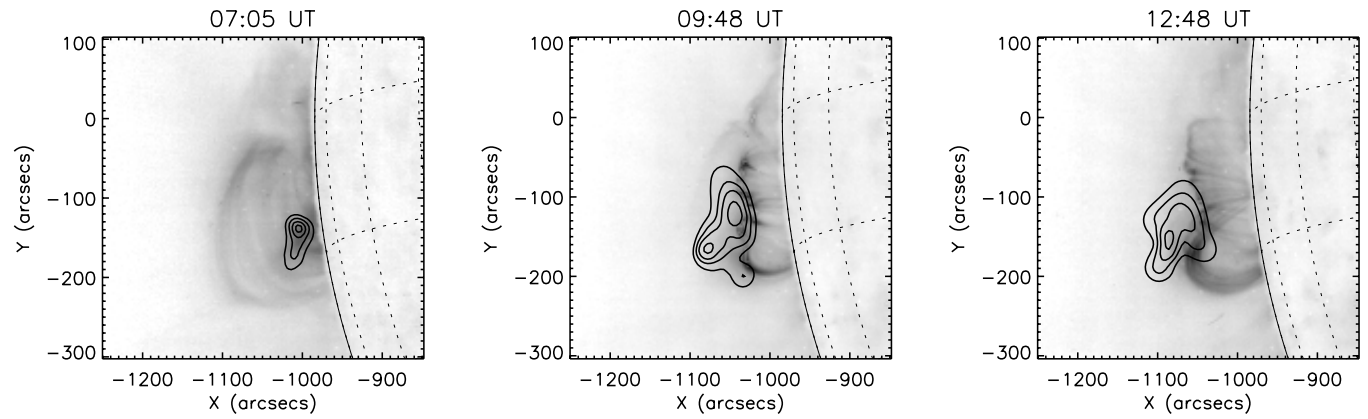

Fig. 13. SoHO/EIT 195 Å images illustrating the decay phase of the 25 January 2007 flare. Contours show the emission in the 7−8 keV range observed with RHESSI.

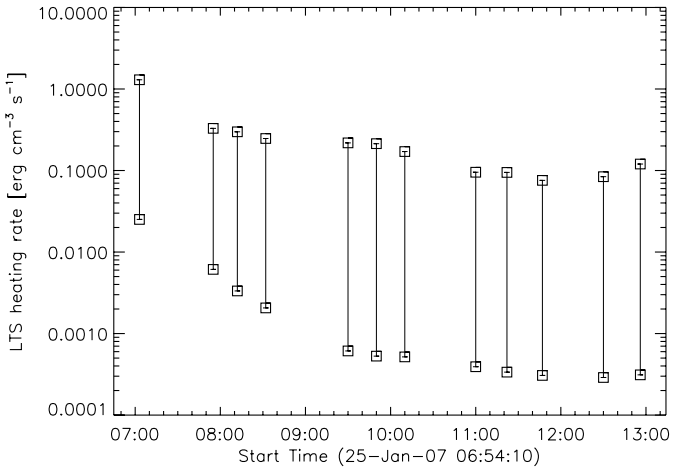

Fig. 14. The 25 January 2007 flare – estimated range of the heating rate of the loop-top source. The real value of the heating must be contained between the upper (upper symbols) and lower (lower symbols) limits of the heating rate.

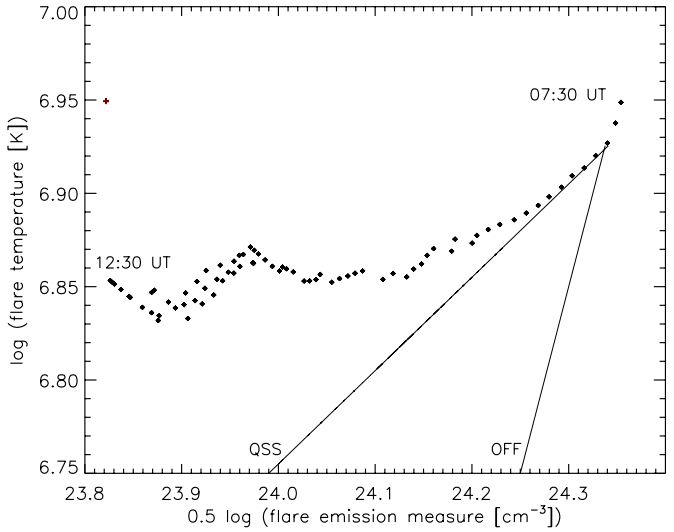

Fig. 15. GOES diagnostic diagram for the 25 January 2007 flare. The OFF and QSS paths of evolution are marked. The flare decay path runs along the QSS path (or even flatter). This confirms non-zero, slowly decreasing heating during the decay phase of the flare.

Table 4. Basic parameters of the loop-top source of the 25 January 2007 flare.

Time [UT]	Size (diameter) [arcsec]	Altitude [10^3 km]	Temperature [MK = 10^6 K]	Emission measure [10^{47} cm^{-3}]
07:03	22.4	30.5	13.3	13.49
07:55	44.4	46.4	12.1	2.83
08:12	42.4	44.8	11.5	1.52
08:32	41.0	50.2	11.1	1.54
09:30	40.6	51.0	10.8	0.75
09:50	37.4	63.3	11.1	0.63
10:10	47.6	55.6	10.8	0.74
11:00	71.2	66.7	10.8	0.44
11:22	55.0	68.6	10.1	0.42
11:47	60.0	72.7	9.9	0.39
12:30	53.0	74.1	9.9	0.36
12:56	51.4	73.2	10.8	0.21

Here we reported three well-observed events. In a future investigation, we will analyse a larger number of flares. Such analysis will give us statistical information on the efficiency of the energy release in LDEs.

Acknowledgements. The RHESSI satellite is a NASA Small Explorer (SMEX) mission. We acknowledge many useful and inspiring discussions with Professor Michał Tomczak. We also thank Barbara Cader-Sroka for editorial remarks and the anonymous referee for useful comments and remarks. This investigation has been supported by a Polish Ministry of Science and High Education, grant No. N203 1937 33.

References

Aschwanden, M. J., Metcalf, T. R., Krucker, S., et al. 2002, Sol. Phys., 219, 149
Carmichael, H. 1963, AAS-NASA Symposium on the Physics of Solar Flares, NASA SP-30, 451
Caspi, A., & Lin, R. P. 2010, ApJ, 725, L161
Czaykowska, A., De Pontieu, B., Alexander, D., & Rank, G. 1999, ApJ, 521, 75
Delaboudinière, J.-P., Artzner, G. E., Brunaud, J., et al. 1995, Sol. Phys., 162, 291
Dere, K. P., Landi, E., Young, P. R., et al. 2009, A&A, 498, 915
Donnelly, R. F., Grubb, R. N., & Cowley, F. C. 1977, NOAA Tech. Memo. ERL SEL-48
Feldman, U., Seely, J. F., Doschek, G. A., & Brown, C. M. 1995, ApJ, 446, 860
Gallagher, P. T., Dennis, B. R., Krucker, S., Schwartz, R. A., & Tolbert, K. 2002, Sol. Phys., 210, 341
Harra-Murnion, L. K., Schmieder, B., van Driel-Gesztelyi, L., et al. 1998, A&A, 337, 911
Hirayama, T. 1974, Sol. Phys., 34, 323

Hirose, S., Uchida, Y., Uemura, S., Yamaguchi, T., & Cable, S. B. 2001, ApJ, 551, 586
Hurford, G. J., Schmahl, E. J., Schwartz, R. A., et al. 2002, Sol. Phys., 210, 61
Isobe, H., Yokoyama, T., Shimojo, M., et al. 2002, ApJ, 566, 528
Jakimiec, J., & Fludra, A. 1992, Adv. Space Res., 11, 99
Jakimiec, J., Sylwester, B., Sylwester, J., Mewe, R., & Peres, G. 1986, Adv. Space Res., 6, 237
Jakimiec, J., Sylwester, B., Sylwester, J., et al. 1987, Sol. Max. Anal. (Utrecht: VNU Science Press), 91
Jakimiec, J., Sylwester, B., Sylwester, J., et al. 1992, A&A, 253, 269
Jakimiec, J., Tomczak, M., Fludra, A., & Falewicz, R. 1997, Adv. Space Res., 20, 2341
Jakimiec, J., Tomczak, M., Falewicz, R., Phillips, K. J. H., & Fludra, A. 1998, A&A, 334, 1112
Jiang, Y. W., Liu, S., Liu, W., & Petrosian, V. 2006, ApJ, 638, 1140
Kahler, S. 1977, ApJ, 214, 891
Karlický, M., & Bárta, M. 2006, ApJ, 647, 1472
Khan, J. I., Fletcher, L., & Nitta, N. V. 2006, A&A, 453, 335
Kołomański, S. 2007a, A&A, 465, 1021
Kołomański, S. 2007b, A&A, 465, 1035
Kontar, E. P., Hannah, I. G., & Bian, N. H. 2011, ApJ, 730, L22
Kopp, R. A., & Pneuman, G. W. 1976, Sol. Phys., 50, 85
Krucker, S., Battaglia, M., Cargill, P. J., et al. 2008, A&ARv, 16, 155
Kundu, M. R., & Grechnev, V. V. 2001, Earth Planets Space, 53, 585
Lin, R. P., Dennis, B. R., Hurford, G. J., et al. 2002, Sol. Phys., 210, 3
Liu, W., Petrosian, V., Dennis, B. R., & Jiang, Y. W. 2008, ApJ, 676, 704
Luciani, J. F., Mora, P., & Virmont, J. 1983, Phys. Rev. Lett., 51, 1664
Masuda, S., Kosugi, T., Sakao, T., & Sato, J. 1998, Observational Plasma Astrophysics: five Years of Yohkoh and Beyond (Kluwer: Academic Publishers), Astrophys. Space Sci. Lib., 229, 259
Nakajima, H., Sato, J., & Fujiki, K. 1998, Solar Physics with Radio Observations, Proceedings of Nobeyama Symposium, NRO Report, 479
Puetter, R. C., & Yahil, A. 1999, Astronomical Data Analysis Software and Systems VIII, ASP Conf. Ser., 172, 307
Phillips, K. J. H., Feldman, U., & Hara, L. K. 2005, ApJ, 634, 641
Phillips, K. J. H., Chifor, C., & Dennis, B. R. 2006, ApJ, 647, 1480
Rosner, R., Tucker, W. H., & Vaiana, G. S. 1978, ApJ, 220, 643
Roy, J.-R., & Datlowe, D. W. 1975, Sol. Phys., 40, 165
Saint-Hilaire, P., Krucker, S., & Lin, R. P. 2009, ApJ, 699, 245
Sheeley, N. R., Bohlin, J. D., Brueckner, G. E., et al. 1975, Sol. Phys., 45, 377
Shibasaki, K. 2002, ApJ, 567, L85
Shibata, K. 1999, Ap&SS, 264, 129
Smith, D. M., Lin, R. P., Turin, P., et al. 2002, Sol. Phys., 210, 33
Sturrock, P. A. 1966, Nature, 211, 695
Sui, L., & Holman, G. D. 2003, ApJ, 596, L251
Sylwester, B., Sylwester, J., Serio, S., et al. 1993, A&A, 267, 586
Uchida, Y., Hirose, S., Cable, S., et al. 1999, PASJ, 51,553
Vorpahl, J. A., Tandberg-Hanssen, E., & Smith, J. B. 1977, ApJ, 212, 550